DOI 10.1007/s11242-011-9838-2

Gas Injection in a Liquid Saturated Porous Medium. Influence of Gas Pressurization and Liquid Films

Clément Louriou · Hanène Ouerfelli · Marc Prat · Mustapha Najjari · Sassi Ben Nasrallah

Abstract We study numerically and experimentally the displacement of a liquid by a gas in a two-dimensional model porous medium. In contrast with previous pore network studies on drainage in porous media, the gas pressurization is fully taken into account. The influence of the gas injection rate on the displacement pattern, breakthrough time and the evolution of the pressure in the gas phase due in part to gas compressibility are investigated. A good agreement is found between the simulations and the experiments as regards the invasion patterns. The agreement is also good on the drainage kinetics when the dynamic liquid films are taken into account.

Keywords Drainage · Porous media · Pore network · Gas pressurization · Gas injection · Thin porous media · Liquid films

1 Introduction

Drainage, i.e., the immiscible displacement of a wetting fluid by a non-wetting one, is probably the most studied and well-understood two-phase flow process in a porous medium. In particular, major advances in the understanding of drainage have been performed thanks to pore network models and experiments on model porous media (Lenormand et al. 1988; Frette

C. Louriou · H. Ouerfelli · M. Prat
Université de Toulouse; INPT, UPS; IMFT, Avenue Camille Soula, 31400 Toulouse, France

C. Louriou · H. Ouerfelli · M. Prat (✉)
CNRS; IMFT, 31400 Toulouse, France
e-mail: prat@imft.fr

H. Ouerfelli · S. B. Nasrallah
Laboratoire d'Eudes des Systèmes Thermiques et Energétiques de Monastir, École nationale d'Ingénieurs de Monastir, 5000 Monastir, Tunisia

M. Najjari
Faculté des Sciences de Gabès, Zirig, 6072 Gabès, Tunisia

et al. 1994; Lovool et al. 2005) and references therein. The main patterns that can be obtained when the displacement depends only on the competition between the viscosity and capillary forces are well summarized by the phase diagram proposed by Lenormand et al. (1988). This diagram involves the capillary number $Ca = \frac{\mu_{\rm nw} U}{\gamma}$, where U is the injection velocity, $\mu_{\rm nw}$ the viscosity of the displacing (non-wetting) phase and γ the interfacial tension between the two fluids and the viscosity ratio $M = \mu_{\rm nw}/\mu_w$, where μ_w is the viscosity of the displaced phase. In this paper, we are interested in the displacement of a liquid by a gas so that $M < 1$. In this case, the invasion pattern changes from a capillary fingering pattern to a viscous fingering pattern as the capillary number, which characterizes the competition between capillary and viscous forces, increases from low values to large values. The patterns can be well simulated using pore network models (Lenormand et al. 1988; Blunt et al. 2002). However, when the displacing fluid is a gas, the question arises as to whether the gas compressibility affects the dynamics of the displacement. It seems that this aspect was neglected in previous studies and is one of the novel aspects brought by the present study.

Gas injection in a porous media is a particular sub-field of drainage, which has also been the subject of many studies, notably in relation with environmental engineering applications such as air sparging in aquifers, e.g. (McCray 2000) or more recently with CO_2 injection issues, e.g. (Dentz and Tartakovsky 2008). In these studies, e.g. (Geistlinger et al. 2006; Stauffer et al. 2009) and references therein, the invasion pattern is greatly affected by gravity effects. The motivation from the present study is somewhat different and explains why gravity effects are not considered. This study can be regarded as a preliminary step to the study of vaporization processes in porous media (Satik and Yortsos 1996) and especially in the porous wicks (Louriou and Prat, accepted), used in cooling devices such as loop heat pipes (Maydanik 2005). Gas pressurization effects are important in the vaporization process, but these wicks are sufficiently thin, a few millimetres thick typically, for gravity effects to be negligible. Thus, our study is of primary interest for thin porous media. The porous layers involved in the proton exchange membrane fuel cells (PEMFC) (Rebai and Prat 2009), paper sheets (Niskanen 1998), porous coatings (Liter and Kaviany 2001) or filtration cakes (Elimelech et al. 1995) are just a few other examples of thin porous media. Yet, the main findings of the present study are of broader interest and also hold in the presence of significant gravity effects. The main restriction is that the pressure in the gas phase is assumed to be spatially uniform (the viscous flow of the gas phase is neglected). This is a reasonable assumption for a thin system, or a pore network of a sufficiently small size, but not when the gas flow develops over large distances, e.g. (Sarrot and Prat 2010). In addition to porous media, it can be also pointed out that this study is of direct interest to microfluidic devices (Squires and Quakes 2005). In contrast with porous media, microfluidic devices are rarely disordered, but the gas pressurization effect and the influence of liquid films reported in our disordered model system would be also present in a system where all the channels are identical.

A somewhat distinguishing feature of the present study is also that the same pore space geometry, i.e., the same realization of the pore network, is used in both the experiments and the simulations. This allows us to compare directly the experimental and numerical results. Of course, it is quasi-impossible to impose exactly the same geometry due to the unavoidable uncertainties due to the fabrication process of experimental model. This will affect the comparison between the experiments and the simulations, but the physical and numerical pore networks are nevertheless sufficiently close to achieve good comparisons.

The situation studied is sketched in Fig. 1. A porous domain, a two-dimensional square network of channels of rectangular cross section in our case, is fully saturated by a wetting liquid initially. Gas is injected laterally through a single injection point located in the middle

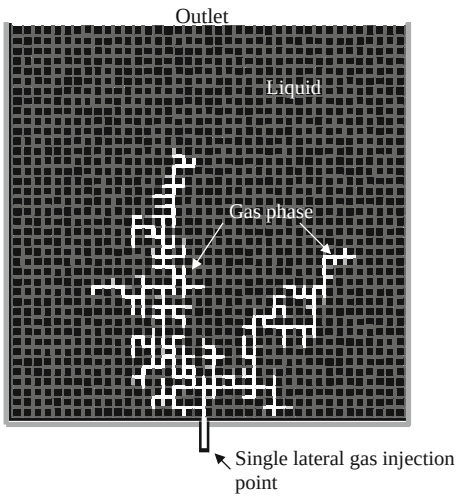

Fig. 1 Schematic of the situation studied

of the injection side (bottom side in Fig. 1). The gas is injected by compressing a certain initial amount of gas connected to the porous medium. The imposed volumetric compression rate is Q_v. The diameter of the injection tube is of the order of a pore size. The liquid can escape only through the side opposite to the injection side (top side in Fig. 1). The lateral sides and the injection side out of the injection tube are impervious. The paper is organized as follows. We begin with the presentation of the model porous medium in Sect. 2. The experimental set-up is described in Sect. 3. The pore network model and the displacement algorithm are presented in Sect. 4. The results are presented and discussed in Sect. 5.

2 Model Porous Medium

The type of model porous medium used in this study is shown in Fig. 2. As in many previous studies, e.g. (Lenormand et al. 1988; Louriou and Prat, accepted), a simple two-dimensional square network is used to represent the pore space. The lattice spacing, i.e., the distance between two neighbour pores, is denoted by a. The throats are channels of rectangular cross section of constant depth e and of width l. The disordered nature of the porous medium lies in the throat widths, which are randomly distributed according to a discrete uniform probability law in the range $[l_{\min}, l_{\max}]$. As shown in Fig. 2, the pores form the junctions of the pore space. A pore, see Fig. 2, is inscribed in a rectangular cuboid of thickness e and of square cross section in the network plane (square in grey in Fig. 2). The width of this square is the width of the widest throat $l_{\max}$. Hence, the length a_{th} of a throat is $a_{\text{th}} = a - l_{\max}$.

The physical porous medium is a 40×40 square pore network of interconnected rectangular channels machined in a Plexiglas plate. The pore network is generated numerically and then machined in the Plexiglas plate thanks to a digitally controlled drilling machine. Except for the uncertainties due to the machining process, the machined pore network is supposedly identical to the pore network used in the numerical simulations. The distance between two pores (lattice spacing a) is 2 mm and the depth e of the channels is uniform and equal to 1mm. The width of the throats is randomly distributed in the range [300, 800 μm] according to a discrete uniform probability law with a 1 μm step. Note however, that the machining is

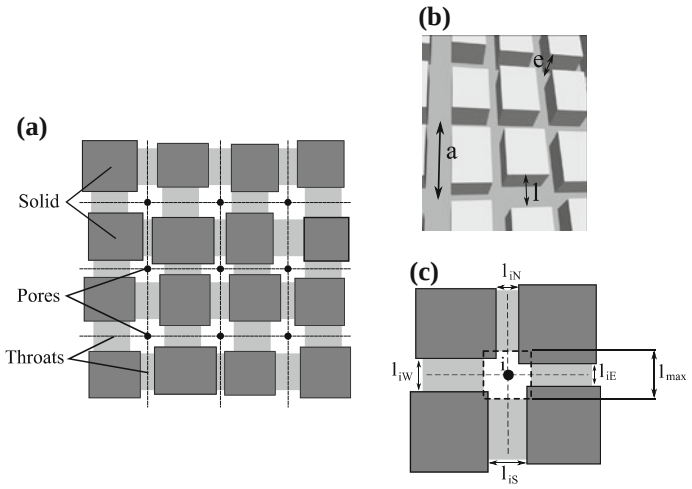

Fig. 2 **a** Sketch of model porous medium. The solid is in *black*, the throats in *gray* and the pores in *white*, **b** detailed view, **c** Pore definition. A square of size equal to the width of the widest throat is used to distinguish the pore and throats

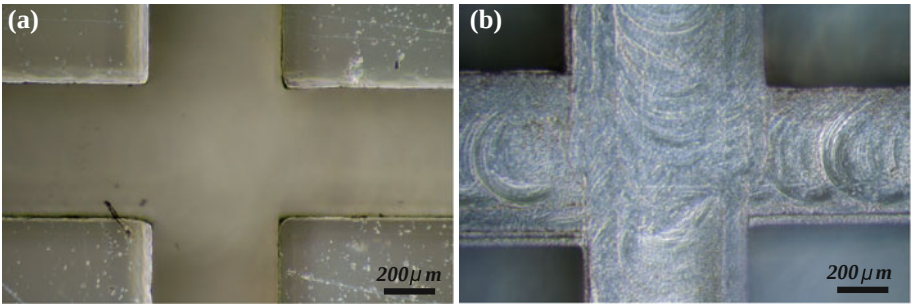

Fig. 3 Microscopy view of the model porous medium

far from perfect and that the uncertainty in the width is estimated to be close to $\pm 10\,\mu$m, thus greater than the increment of $1\,\mu$m between two successive sizes in the width distribution law. This does not lead to major problems, except at very low capillary numbers however, in the comparison with the simulation as discussed in Sect. 5. To avoid undesirable gravity effects, the channel size must be lower than the capillary length. This sets the upper bound of about 1mm. An additional channel is machined to link the gas inlet pore to the injection tube, which, as sketched in Fig. 4, is a syringe needle. A transparent Plexiglas cover plate is set on top of this system and fixed with nine equally spaced and controlled clamping screws. The side of the cover plate in contact with the machined network is carpeted with a layer of Rhodorsil RTV (a transparent silicone resin) for tightness. One can refer to Chapuis (2006) for more details. To check the machining quality, the machined network has been observed with a microscope. Figure 3 presents two magnified views of a pore. As can be seen, the quality of the machining is good. The edges are clean and straight. Small-scale grooves due to the machining process are, however, visible.

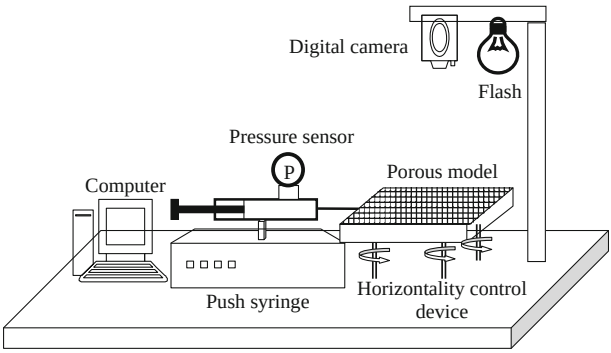

Fig. 4 Schematic of experimental set-up

3 Experimental Set-Up

The wetting fluid is silicon oil (Rhodorsil 47V200) with a viscosity of 0.1795 Pa.s and an interfacial tension of 0.021 N/m. The non-wetting fluid is always air. The properties of the silicon oil have been measured at the temperature of the experiment room (22°C).

As sketched in Fig. 4, the gas is injected thanks to a plastic syringe connected to a syringe driver system pushing the plunger of the syringe forward at an accurately controlled rate (we use a '11'Plus, Harvard Apparatus). A pressure transducer (Keller Series 41X with a precision of ± 10 Pa) is connected to the syringe so as to monitor the gas pressure evolution in the syringe chamber. The evolution of the gas cluster in the network, placed horizontally, is recorded with a Nikon D60 camera set above the system. Images of the phase distribution are taken every second.

The experimental procedure is as follows: (1) the porous model is saturated with degassed oil using a vacuum pump, (2) the porous model is placed horizontally and is connected to the syringe, (3) drainage starts using the constant volumetric compression rate injection mode of the push syringe, and the data acquisition procedure is launched thanks to a PC connected to the camera and the pressure transducer. The experiment stops when the gas reaches the outlet (breakthrough). The initial volume of gas (in the syringe, tubing and pressure transducer) is $5.5\,\mathrm{cm}^3$.

4 Pore Network Model

As mentioned before, the same network geometry is, as much as possible, imposed in the simulations and in the experiments. In accordance with the experiments, gravity effects are neglected, and the liquid is supposed to be perfectly wetting.

The drainage dynamics in our situation can be described qualitatively as follows. As a result of the imposed gas injection volumetric flow rate Q_V, the pressure increases in the gas (located in the syringe and in the porous medium), which is considered as a compressible ideal gas. When the increase in the pressure is sufficient, some menisci can start moving in the porous medium. This induces a liquid flow and therefore the generation of a pressure field in the liquid. Because of viscous effects in the liquid, the throats and pores that become invadable by the gas cannot be drained instantaneously. Thus, the pressure in the gas phase can continue to increase during the invasion. The principle of the algorithm is essentially to

express that the drainage time of the invaded throats and pores should be equal to the time needed for the gas to replace the liquid in the pores and throats where a meniscus is moving. These phenomena are taken into account in the algorithm described hereafter, assuming a spatially uniform pressure P_g at any time in the gas phase. To the best of our knowledge, the type of algorithm described below was first proposed in Satik and Yortsos (1996), but for a more involved situation of vaporization and without the consideration of liquid films.

4.1 Flow Model

The viscous flow is therefore computed only in the incompressible liquid phase. The viscous pressure drop is neglected in pores, which serve mainly as liquid reservoirs, and therefore taken into account only in the throats. Flow in a throat is laminar and described by Hagen–Poiseuille law. The flow in a throat is therefore expressed as

$$q_{ij} = \frac{g_{ij}}{\mu} \Delta P_{ij} \tag{1}$$

where q_{ij} is the flow rate in the ijth throat, μ is the liquid viscosity, ΔP_{ij} is the pressure drop across the throat (= the pressure difference between the two pores adjacent to the throat). In Eq. (1), g_{ij} is the throat hydraulic conductance, which is expressed as

$$g_{ij} = \frac{2 S_{ij} k_{ij}}{a} \tag{2}$$

where S_{ij} is the throat cross section and $k_{ij} = \frac{2}{Po_{ij}} \left[\frac{l_{ij} e}{l_{ij} + e} \right]^2$, where the Poiseuille number Po_{ij} is given by $Po_{ij} = 14.227 + 1402.5 \left(\frac{1 + r^* (\sqrt{2} - 1)}{4(1 + r^*)} - \frac{\sqrt{2}}{8} \right)^{1.9}$ according to Tirunarayanan and Ramachandran (1965), r^* is the aspect ratio: $r^* = \frac{l_{ij}}{e}$.

Mass conservation at each pore required

$$\sum_j q_{ij} = 0. \tag{3}$$

where the sum runs over the four throats connected to pore i. The system of equations (3) is solved numerically using a conjugate gradient method.

Capillarity is taken into account through the Young–Laplace equation assuming a perfectly wetting liquid (contact angle ≈ 0). Hence, the capillary pressure threshold of a throat, that is the pressure difference across a meniscus located at the entrance of a throat that must be exceeded for the throat to be invaded by the gas, is expressed as,

$$P_c \approx \sigma \left(\frac{2}{e} + \frac{2}{l} \right) \tag{4}$$

The initial and boundary conditions are specified so as to be in accordance with the experiments. A constant gas mass m, equal to the total mass contained in the syringe at $t = 0$, is considered and a constant compression rate Q_v is imposed. A constant pressure, equal to the atmospheric pressure, is imposed at the outlet, whereas all other sides are subjected to no-flow boundary condition.

Three situations can be distinguished as regards the boundary condition at a meniscus in the pore network:

i. *The meniscus is in a pore:* We assume for simplicity that a meniscus in a pore is always moving. The pressure in the liquid at such a meniscus present at the inlet or into a pore

is imposed equal to the gas pressure lowered by the pore capillary pressure threshold $P_c \approx \frac{2\sigma}{e}$ (although the in-plane curvature radius of a meniscus present in a pore is not much larger than in a throat in the model porous medium considered in this study, the in-plane curvature radius in a pore is neglected).

ii. *The meniscus is in a throat or at the entrance of a throat and can move:* This situation occurs when $P_g \geq P_\ell + P_c$, where P_ℓ is the liquid pressure at the meniscus. In that case, the pressure of the liquid at the meniscus is imposed equal to $P_\ell = P_g - P_c$. The pressure P_p in the adjacent liquid pore is then computed as $P_p = P_g - P_c - \Delta P$, where ΔP is the viscous pressure drop between the meniscus and the pore. The position of the meniscus in the throat is updated at each step of the computation as functions of throat filling rate and throat volume. Such a throat is referred to as an invadable throat.

iii. *The meniscus is in a throat or at the entrance of a throat and cannot move:* This situation occurs when $P_g \leq P_\ell + P_c$. In that case, no flow is possible in the throat, and a zero flow rate condition is imposed in that throat.

4.2 Liquid Films

As evoked in the Introduction, drainage dynamic liquid films have a non-negligible influence on drainage time. As sketched in Fig. 5, dynamic liquid films refer to the liquid film left behind a moving meniscus. The consequence of liquid films is twofold: (1) the volume of liquid drained in a throat is less than in the absence of films since a fraction of the liquid stays along the walls of the throat, (2) the cross-section area in a throat available for the gas invasion is diminished. This impacts the throat gas filling time since the volume available for the gas invasion is less. A simple approach is used to deal with liquid films, i.e., to estimate the volume fraction of an invaded pore or throat occupied by liquid films.

In a channel of circular cross section, one can rely on the classical relationship developed by Bretherthon (Bretherton 1960) for estimating the film thickness as a function of the capillary number. The case of channels of square /rectangular cross section has been also studied (Wong et al. 1992a,b) (quasi-static limit) (Wong et al. 1995a,b; Kolb and Cerro 1991) (dynamic films). Here, we make use of the results presented in Kolb and Cerro (1991). Two regimes are distinguished: one with axisymmetric menisci for high capillaries numbers and the other with non-axisymmetric menisci for lower capillaries numbers. In our study, the capillary number is most of the time lower than 0.1, which corresponds to non-axisymmetric menisci. The maximal volume fraction occupied by the liquid films in a throat or a pore in this regime is 0.3 and corresponds to a capillary number of 0.1.

From their experimental results, Kolb and Cerro plotted the evolution of the channel volume fraction ε_f occupied by the liquid films as a function of the capillary number [see Figure 10 in Kolb and Cerro (1991)]. In our case, the capillary number cannot be readily estimate from the compression rate Q_v because of compressibility effects. For simplicity,

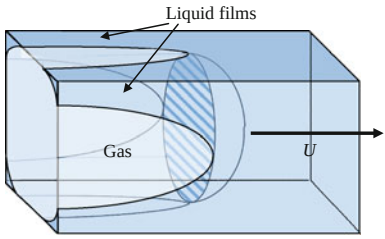

Fig. 5 Dynamic liquid films. The relative motion between the solid and the meniscus leads to the deposition of a liquid film on the pore walls

we have nevertheless directly used their results estimating the capillary number based on the liquid viscosity as $Ca_\ell = \frac{\mu_\ell U}{\gamma}$ with $U = \frac{Q_V}{S}$, where S is the cross-section area of the network and μ_ℓ the liquid dynamic viscosity. From the estimate of Ca_ℓ, the value of ε_f is read on Kolb and Cerro plot and imposes in all throats and pores invaded by the gas. Thus for a given compression rate Q_V, a constant ε_f is imposed in the simulation. The procedure has been tested from experiments with a single square capillary tube, as well as for a circular tube (using Bretherthon' formula in this case), and a very good agreement was found between the experiments and the computations (Louriou 2010).

To end this section, it should be pointed out that the results reported in Kolb and Cerro (1991) show that the volume of liquid in a channel associated with the dynamic films is at least twice the volume of static films, i.e. (Wong et al. 1992b).

4.3 Displacement Algorithm

In our simulations, several throats and pores can be drained simultaneously. The algorithm is sketched in Fig. 6 and can be summarized as follows:

1. Initialization: All throats and pores are supposed saturated with oil except the pore at the inlet where gas injection takes place.
2. Pressurization: In this step, the menisci are not mobile. The pressure increases up to the value where a first invasion becomes possible. Hence, the first throat to be invaded and the associated minimum gas pressure needed to overcome the invasion capillary pressure threshold of this throat are determined.
3. Filling: The time needed for fully invading a throat or a pore is found. Hence, the gas pressure level needed to invade fully a pore or a throat is determined. This step implies iterations on the gas pressure. For each iteration, new invadable throats can be detected. Thus, in this step, only one pore (or throat) is completely drained, but many can be partially drained.
4. Test: A test is performed so as to determine whether the current gas pressure is high enough for invading new throats (or pores). Computation returns to step 3 if yes and to step 2 if not.
5. Computation stops when the gas reaches a pore at the outlet.

Further details on the pressurization and filling steps are now given.

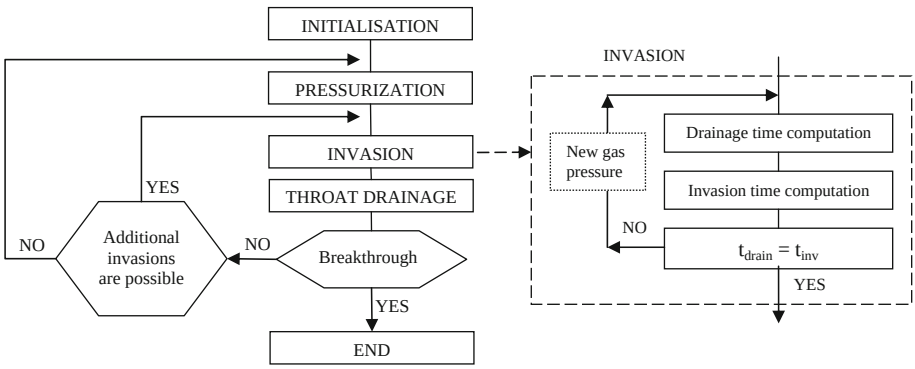

Fig. 6 Displacement simulation algorithm

Pressurization step: This step is used to determine the gas pressure needed to induce a flow in at least one pore or throat. This pressure is given by $P_{\mathrm{g\,min}} = \min(P_{c_{ij}} + P_{\mathrm{int\_}j})$, where $P_{\mathrm{int\_}j}$ is the pressure in the liquid in the pore adjacent to the meniscus, i and j run over all the throats where a meniscus is present. Then from the volume occupied by the gas and the initial gas mass, the time needed to reach this gas pressure is determined,

$$t_{\mathrm{pressurization}} = \frac{\Delta V}{Q_V} \tag{5}$$

where we recall that Q_V is the imposed gas injection volumetric flow rate and ΔV is the volume of gas that must be compressed to reach the pressure $P_{\mathrm{g\,min}}$,

$$\Delta V = V_{\mathrm{g}} - V(P_{\mathrm{g\,min}}) \tag{6}$$

where V_{g} is the volume of gas at the beginning of the considered pressurization step. $V(P_{\mathrm{g\,min}})$ is the volume of gas corresponding to the pressure $P_{\mathrm{g\,min}}$ and is determined using the ideal gas law,

$$V(P_{\mathrm{g\,min}}) = \frac{mRT}{P_{\mathrm{g\,min}}M} \tag{7}$$

where m is the total mass of gas in the system, R is the ideal gas constant, T is the temperature and M the molar mass.

Filling step: In this step, the time needed for the gas to completely fill a throat (or pore) is determined. This time corresponds to the time needed for the liquid to completely leave a throat (or pore). The main idea of the invasion algorithm is thus to equal two times, the time spent by the liquid to leave the throat (or pore) (this time is referred to as the 'drainage time') and the time spent by the gas to fill it (this time is referred to as the 'invasion time').

Drainage time: This time is computed from the volumetric flow rate leaving the throat or the pore to drain, which is obtained from solving numerically Eq. (3). For a pore (containing a volume of liquid V_{pi})

$$t_{\mathrm{drain\_}i} = \frac{V_{pi}}{\sum_j q_{ij}} \tag{8}$$

where j runs over all pores adjacent to pore i and occupied by liquid. For a throat (containing a volume of liquid V_{ij})

$$t_{\mathrm{drain\_}ij} = \frac{V_{ij}}{q_{ij}} \tag{9}$$

Since many pores and throats can be invaded simultaneously, the drainage time corresponds to the minimum time computed from Eqs. (8) and (9),

$$t_{\mathrm{drain}} = \min(t_{\mathrm{drain\_}i}, t_{\mathrm{drain\_}ij}) \tag{10}$$

Invasion time: The ideal gas law is used here in the same way as in the pressurization step. The aim is to found the time required to maintain the pressure computed in the previous step (pressurization step) once the gas volume has increased due to the filling of new throats (or pores). As in the pressurization step, the invasion time is expressed as a function of the compression rate as

$$t_{\text{inv}} = \frac{\Delta V}{Q_V} \tag{11}$$

where $\Delta V = V_{\text{g}}^{+} \sum V_{\text{throats}} + \sum V_{\text{pores}} - V_{\text{g}}(P_{\text{g min}})$, V_{g} is the volume of gas at the beginning of the filling step, $\sum V_{\text{throats}}$ and $\sum V_{\text{pores}}$ are the sums of the volumes filled in all the throats and pores that are partially drained during t_{drain}, $V_{\text{g}}(P_{\text{g min}})$ is the volume of gas corresponding to gas pressure $P_{\text{g min}}$ (Eq. 7).

Iterations: The two times are considered to be equal when Eq. (12) is satisfied,

$$\frac{|t_{\text{drain}} - t_{\text{inv}}|}{t_{\text{drain}}} \leq \varepsilon \tag{12}$$

In Eq. (12), ε is a convergence parameter and tests have shown that $\varepsilon = 10^{-7}$ leads to good results, i.e., using a smaller ε does not modify the results. Iterations over the gas pressure are necessary to satisfy Eq. (12). The gas pressure is the only parameter driving the drainage dynamics. Increasing the gas pressure means decreasing the drainage time and increasing the invasion time. Decreasing the gas pressure has exactly the opposite effect.

After each iteration, new throats or pores can become invadable because of the change in the pressure. It may also happen that some pores and throats that were invadable cease to be invadable. It is thus necessary to determine the throats and pores that can be invaded after each iteration on the gas pressure during the filling step.

4.4 Trapped Clusters, Fragmentation

A trapped cluster is a group of liquid pores and throats completely surrounded by the gas phase and therefore not connected to the outlet. Trapped clusters can form as a result of the invasion process. Since the gas pressure is spatially uniform at any times in this model, no invasion can take place in a trapped cluster.

As reported for example in Vedvik et al. (1998), a throat invaded by the gas can be reinvaded by the liquid at a later stage of the displacement because of snap-off phenomena, see Vedvik et al. (1998) for more details. This leads to the fragmentation of the invading gas cluster. This phenomenon is, however, not observed in our experiments and therefore not taken into account.

5 Results and Discussion

The objective is to study the influence of the imposed volumetric compression rate Q_v on the evolution of gas pressure P_{g} and invasion pattern. As usual for drainage, various cases are distinguished depending on the value of capillary number. As mentioned before, the capillary number cannot be truly specified a priori since we do not know in advance the flow rate resulting from the compression of the gas mass in the system. A reasonable estimate is given by $Ca = \frac{\mu_g U}{\gamma}$ with $U = \frac{Q_V}{S}$, where S is the cross-section area of the network.

5.1 Low Capillary Number

With a volumetric compression rate of 0.1ml/hr, the capillary number is 4.5×10^{-8}. For such a low value of the capillary number, the displacement is expected to be controlled by capillary effects only and a capillary fingering pattern is expected (Lenormand et al. 1988).

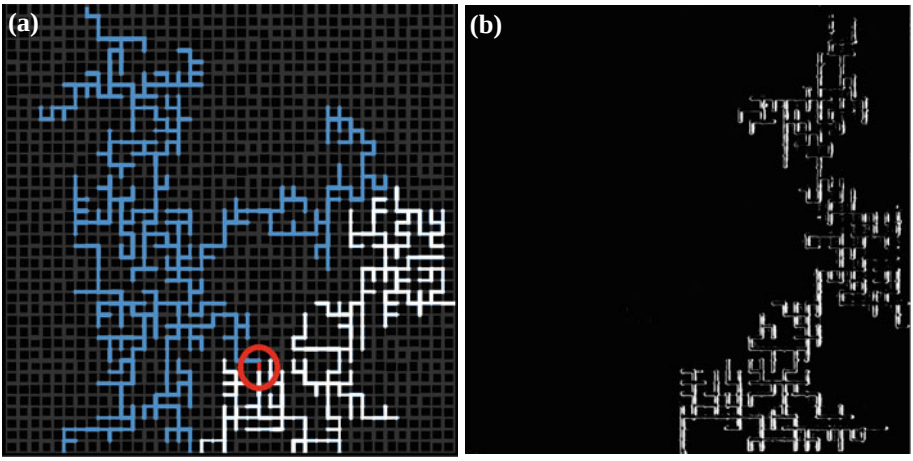

Fig. 7 Drainage at 0.1 ml/h. **a** Numerical simulation, **b** experimental snapshot

Comparison between the experimental and numerical pattern at breakthrough is presented in Fig. 7.

At first glance, the numerical and experimental patterns seem completely different. In particular, a much greater fraction of the pore space is invaded at breakthrough in the simulation. A more detailed inspection reveals, however, that the difference originates from one throat (shown in a circle in Fig. 7a). This throat is invaded in the simulation, but not in the experiment. This throat opens the region on the left visited in the simulation. Interestingly, the region (shown in white in Fig. 7a) invaded in the simulation before invasion of this "sensitive" throat is essentially identical to the region invaded in the experiment. The invasion is controlled by capillary effects only is in this limit, that is by the throat sizes (according to the invasion percolation algorithm (Wilkinson and Willemsen 1983), which describes well this regime, the throat of largest width available along the liquid–gas interface is selected at each step of the invasion). As a result, a slight difference between two throats of approximately the same size between the experimental model and the numerical network is sufficient to modify the invasion pattern.

Owing to the uncertainties associated with the machining process, such a difference in the hierarchy of throat capillary thresholds between the experiment and the simulation is not surprising. The capillary pressure threshold of the 'sensitive' throat can also be greater than expected because of a defect (impurity or a residual tiny piece of Plexiglas for example). It should be also pointed out that many throats have the same width (to the machine precision) in the simulation (we recall that a throat size discrete probably law is used). This is not the case in the experiment due to the errors introduced by the machining. The invasion is, however, performed one throat at the time in the simulation (see Fig. 8) and the choice between widest throats of exactly the same size (to the machine precision) along the interface is in fact dictated by the slight pressure variations in the liquid due to the viscous effects (even though these pressure variations in the liquid are very small compared to the throat capillary pressure thresholds). This suggests that a throat size distribution where all throats have a different size is certainly better adapted to perform the comparison between experiments and simulations in this regime.

An obvious idea from Fig. 7 is to modify the size of the sensitive throat to get a better agreement with the experiment. This works for a while and then a new 'sensitive' throat is

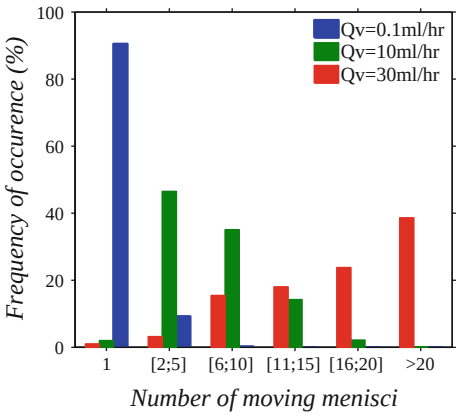

Fig. 8 Number of moving menisci. The histograms are obtained as follows. For a given compression rate, the number of moving menisci N_{mm} is determined for each step of the displacement, i.e., each time a pore or a throat becomes fully invaded by the gas (in the bulk only since a fraction of the pore or throat volume is occupied by liquid films). A histogram in the Figure corresponds to the statistic of N_{mm} at the end of displacement

found along the invasion path, leading again to difference in the experimental pattern and the numerical ones. This shows again that the invasion pattern is quite sensitive to the tiny details affecting the size of the 'sensitive' throats. This is particularly important if one is interested in predicting the invasion pattern for a particular realization as here (for example, the accuracy of pore and throat sizes determined from X-ray tomography of a real sample is likely to be not sufficient to expect a perfect agreement between a simulation and an experiment in the regime dominated by capillary forces). However, one is often more interested in statistical properties obtained over a large number of realizations. These statistical properties are not affected by the existence of these sensitive throats. Also, it can be noticed that this regime has been the object of many previous studies and is characterized by a somewhat classical pressure evolution (see below). It is therefore somewhat less interesting than the two other regimes considered in the following in the context of the present paper.

The evolution of the pressure, using the atmospheric pressure in the laboratory as reference pressure P_{ref}, is depicted in Fig. 9 (hence the pressure shown in Fig. 9 is $P_{\mathrm{g}} - P_{\mathrm{ref}}$). The curves are shown up to the breakthrough (t_{BTexp}) in the experiment. The breakthrough time is obviously greater in the simulation since a larger fraction of the network is invaded, but the evolution of the pressure for $t > t_{\mathrm{BTexp}}$ is not different from the one shown in Fig. 9 after the initial pressure peak. The percolation capillary pressure threshold corresponds to a throat of width $l = 0.550\,\mathrm{mm}$. According to Eq. (4), this gives for the used oil $P_c \approx 118\,\mathrm{Pa}$ (for which the surface tension $\sigma \approx 21 \times 10^{-3}\,\mathrm{N/m}$), whereas the range of capillary pressure thresholds is [94.5 Pa ($l = 0.8\,\mathrm{mm}$) −181 Pa ($l = 0.3\,\mathrm{mm}$)]. As can be seen from Fig. 9, the gas pressure fluctuates around the percolation capillary pressure threshold (except at the very beginning where the gas pressurization effect is clearly visible), which is the expected behaviour in the IP regime. Thus, there is no significant overpressure in the growing gas cluster (except at the beginning). The agreement between the simulations and the experiments is good although the amplitude of the pressure variations in the IP regime is somewhat greater in the simulation. As can be seen, there is, however, a significant overpressurization of the gas at the very beginning of the invasion, this initial phase being somewhat longer in the simulation. This effect is much more marked when the capillary number is increased as discussed hereafter. Also, we recall in passing that this type of information, i.e., the pressure fluctuations, can be useful to characterize the pore space of a porous medium, e.g (Yuan and Swanson 1989).

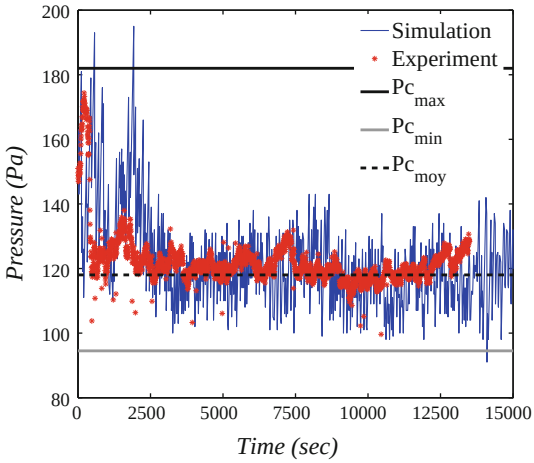

Fig. 9 Numerical and experimental pressure curves for drainage at 0.1 ml/h

5.2 Intermediate Capillary Number

The results obtained with an inlet flow rate of 10ml/hr ($Ca \approx 4.5 \times 10^{-6}$) are presented and discussed in this section. In this regime, both capillary and viscous effects are important and a transition towards a viscous fingering pattern is expected (Lenormand et al. 1988). As illustrated in Fig. 8, the process of multiple invasions (Cottin et al. 2010) becomes common in this regime. Between 2 and 5 throats are simultaneously invaded about every two steps and up to 20 simultaneous throat invasions occur in some steps of the displacement. The invasion pattern in both the simulation and the experiment is shown in Fig. 10 at various stages of invasion. The elapsed time between two successive series of images is 15 s. As a result of viscous effects in the liquid, the pressure decreases in the liquid on average in the main direction of the displacement. This favours invasion in the main direction of the flow and leads to an elongated pattern in the later stages of the invasion as can be clearly seen from Fig. 10.

The agreement between the simulation and the experiment is quite good. It should be pointed out that the patterns are compared at the same times. Thus, the comparison is good not only in terms of pattern but also in terms of invasion kinetics. A detailed comparison of images 1–4 is proposed in Fig. 11. Several remarks can be made. Throat partial invasions are considered in the simulation. The partially invaded throats are shown in grey in the simulation patterns. The darker a grey throat, the lower its partial filling. Interestingly, partially invaded throats are also visible in the experiment snapshots (on top of images # 1 for example). Second, as for the comparison for the low capillary number, some throats that are invaded in the simulation are not in the experiment (see for example images # 4). Explanations are similar to the ones given in Sect. 5.3. However, the impact on the whole pattern is quite limited. Liquid re-invasion of some throats and pores is observed in the experiment (compare the region near the injection pore between images # 1b and #4b). This phenomenon is not taken into account in the simulation and can be explained by the decrease in the gas pressure during the displacement (see Fig. 12 which is commented below).

The evolution of gas pressure in both the experiment and the simulations is shown in Fig. 12.

There is a significant pressure peak at the beginning followed by a progressive decrease of the mean gas pressure. The evolution of the pressure is significantly different from the

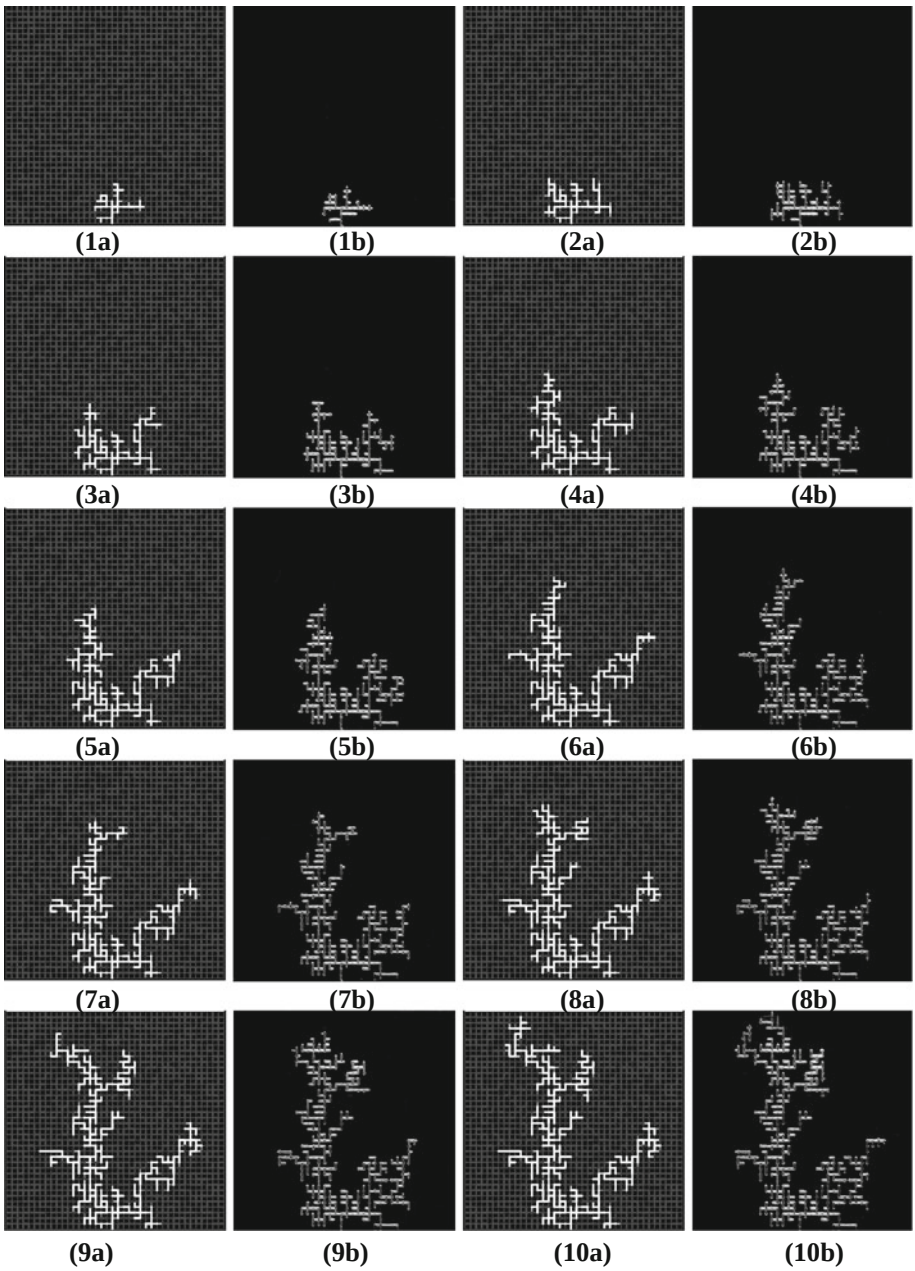

Fig. 10 Invasion pattern for $Q_v = 10\,\text{ml/h}$. Figures are numbered from 1 to 10 in chronological order, the suffix a is for the numerical pictures and the suffix b for the experimental snapshots. The elapsed time between each group of two images is 15 s

low capillary case (Fig. 9). There is a significant gas pressurization effect. Then, the pressure remains significantly higher than the pressure corresponding to the percolation capillary pressure threshold ($P_c \approx 118\,\text{Pa}$), but this is due in part to the variation of the pressure in the

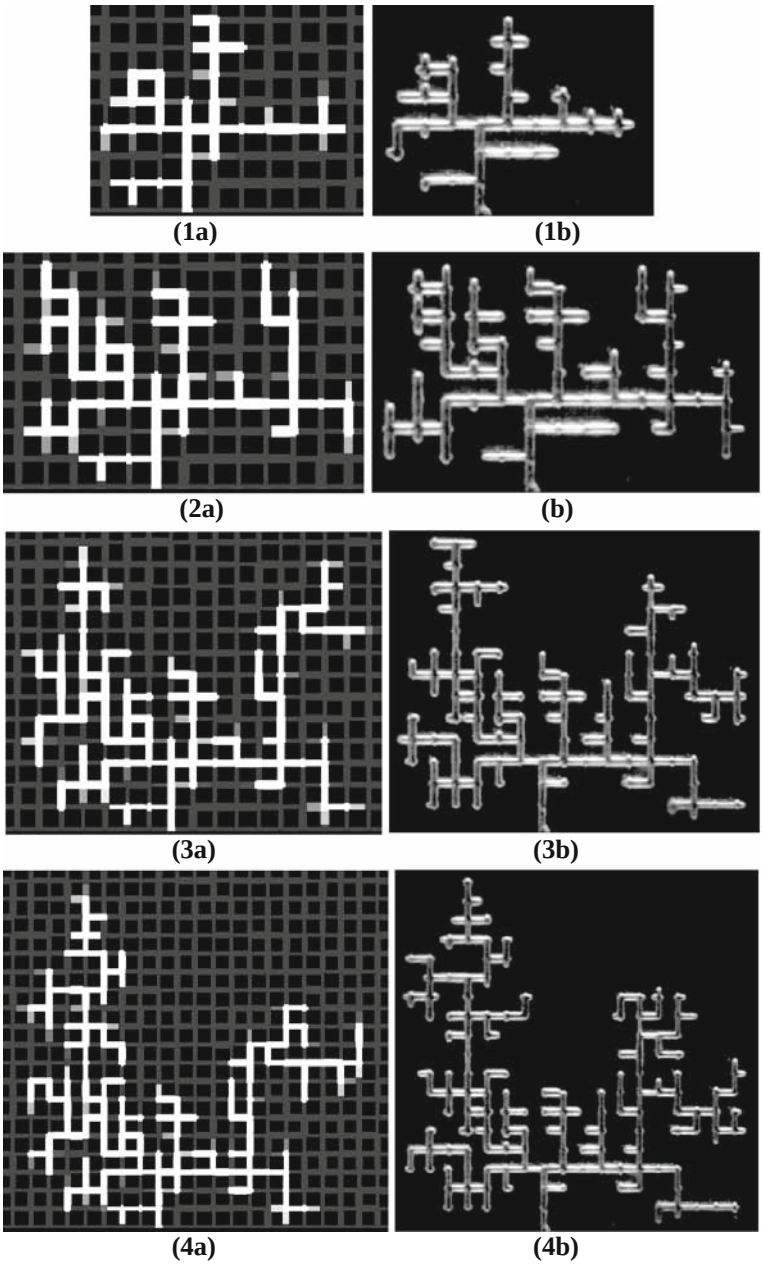

Fig. 11 Detailed comparison of Figs. 1–4 of Fig. 10. The elapsed time between each group of two images is 15 s

liquid due to the viscous pressure drops. The numerical and experimental curves are in very good agreement during the first half of the displacement. The comparison for the second half up to breakthrough indicates that a much better agreement is found when the liquid films are taken into account in the simulations. As for a single capillary tube (Louriou 2010), for which the agreement between the model and the experiment was still better, the consideration of the

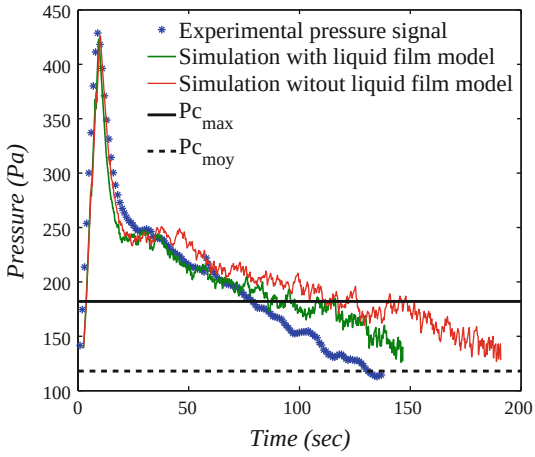

Fig. 12 Numerical and experimental pressure curves for drainage at 10 ml/h

liquid films is crucial to predict a breakthrough time comparable to the experimental time. As illustrated in Fig. 12, neglecting the liquid films leads to a significantly greater breakthrough time since more liquid must be displaced. The liquid films do not affect, however, the pressure peak at the beginning of the displacement.

5.3 High Capillary Number

When the capillary number is further increased (i.e. the volumetric compression rate Q_v in our case), the invasion becomes essentially controlled by the pressure variations in the liquid due the induced viscous flow. As shown in Fig. 8, there are more and more menisci moving simultaneously as the capillary number increases and the invasion pattern tends to become more and more elongated along the main direction of the flow. This is illustrated in Fig. 13, which shows again a good agreement between the experiment and the simulation.

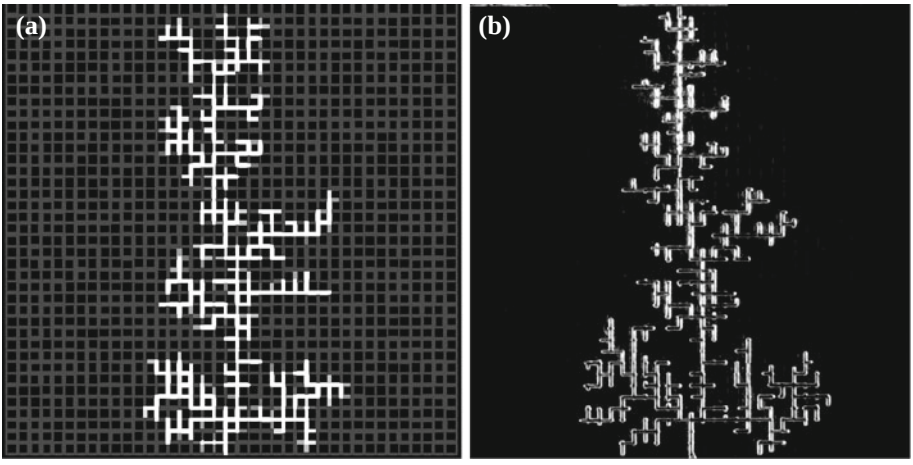

Fig. 13 Drainage at 30 ml/h ($Ca \approx 1.5 \times 10^{-5}$). Pattern at breakthrough. **a** Numerical picture, **b** experimental snapshot

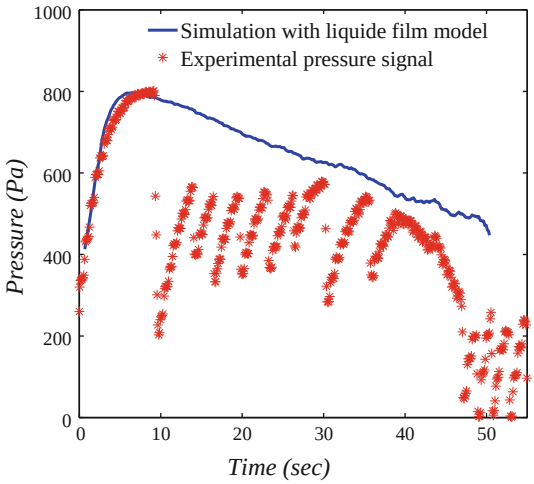

Fig. 14 Numerical and experimental pressure curves for drainage at 30 ml/h ($Ca = 1.5 \times 10^{-5}$)

The pressure curves, depicted in Fig. 14, are in very good agreement during the initial pressurization stage, with a pressure peak up to 800 Pa. After this peak, a gas leak near the pressure transducer, although not affecting the invasion dynamics, altered the pressure measurement as can be seen from Fig. 14. This is unfortunate but nevertheless, it can be also clearly concluded from Fig. 14 that the breakthrough times ($\approx$ 50 s) are in very good agreement between the experiment and the simulation.

6 Conclusion

In this paper, we developed a pore network model of gas injection into a liquid saturated porous medium taking into account the gas pressurization effect and the liquid films remaining along the pore walls behind moving menisci.

Comparisons were performed with experiments with a physical network as much as possible identical, in the limits of our fabrication device, to the numerical one. The agreement between the experiments and the simulations was satisfactory, not only in terms of invasion patterns but also in terms of drainage kinetics.

Our results indicate a significant pressurization of the gas phase in the early stages of the invasion. The pressure peak increases with the capillary number. It is thus necessary to take into account this phenomenon for a correct prediction of drainage kinetics.

The liquid films also affect the drainage dynamics and must therefore be included in the model for predicting the drainage kinetics.

A major limiting assumption of the model is that the gas pressure is supposed spatially uniform at any time. Hence, the viscous flow in the gas phase is neglected. This is acceptable for sufficiently small networks (thin systems) as considered in this paper but not when the gas flow develops of large distances or in the presence of a sufficiently high thermal gradient for example (Louriou and Prat, accepted). It would be therefore interesting to improve the model so as to take into account both the gas compressibility and the viscous flow in the gas.

Also, additional phenomena, such as the fragmentation phenomenon of invading gas cluster or, as observed in our experiments, liquid re-invasion effects when the gas pressure

decreases, not seen or of marginal impacts in our case may become more important for larger networks.

Acknowledgments Financial supports from CNES and Région Midi-Pyrénées are gratefully acknowledged.

References

Blunt, M., Jackson, M., Piri, M., Valance, P.: Detailed physics, predictive capabilities and macroscopic consequences for pore network models of multiphase flow. Adv. Water Res. **25**, 1069–1089 (2002)

Bretherton, F.P.: The motion of long bubbles in tubes. J. Fluid Mech. **10**, 166–188 (1960)

Chapuis, O.: Influence des conditions de mouillage sur les déplacements quasi-statiques eau-air et l'évaporation en milieux poreux modèles., PhD thesis, INPT (in French, 2006)

Cottin, C., Bodiguel, H., Colin, A.: Drainage in two-dimensional porous media: from capillary fingering to viscous flow. Phys. Rev. E **82**(4), 046315 (2010)

Dentz, M., Tartakovsky, D.M.: Abrupt-interface solution for carbon dioxide injection into porous media. Transp. Porous Media **79**(1), 15–27 (2008)

Elimelech, M., Gregory, J., Jia, X., Williams, R.: Particle Deposition & Aggregation. Butterworth-Heineman, Oxford (1995)

Frette, V., Feder, J., Jossang, T., Meakin, P., Maloy, K.J.: Fast, immiscible fluid-fluid displacement in three-dimensional porous media at finite viscosity contrast. Phys. Rev. E **50**, 2881 (1994)

Geistlinger, H., Krauss, G., Lazik, D., Luckner, L.: Direct gas injection into saturated glass beads: transition form incoherent to coherent gas flow pattern. Water Resour Res. **42**, W07403 (2006)

Kolb, W.B., Cerro, R.L.: Coating the inside of a capillary of square cross section. Chem. Eng. Sci. **46**(9), 2181–2195 (1991)

Lenormand, R., Touboul, E., Zarcone, C.: Numerical models and experiments on immiscible displacements in porous media. J. Fluid Mech. **189**, 165–187 (1988)

Liter, S.G., Kaviany, M.: Pool-boiling CHF enhancement by modulated porous-layer coating. Theory and Experiment. Int. J. Heat Mass Transf. **44**, 4287–4311 (2001)

Louriou, C.: Modélisation instationnaire des transferts de masse et de chaleur au sein des évaporateurs capillaires. PhD thesis (in French), INPT, (2010)

Louriou, C., Prat, M.: Experimental and numerical pore network study of bubble growth by vaporisation in a porous medium heated laterally. Accepted for publication in Int. J. Therm. Sci.

Lovool, G., Méheust, Y., Maloy, K.J., Aker, E., Schmittbuhl, J.: Competition of gravity, capillarity and viscous forces during drainage in two dimensional porous medium, a pore scale study. Energy **30**, 861–872 (2005)

Maydanik, Y.: Loop heat pipes. Appl. Therm. Eng. **25**, 635–657 (2005)

McCray, J.E.: Mathematical modeling of air sparging for subsurface remediation: state of the art. J. Hazard Mat. **72**, 237–263 (2000)

Niskanen, K. (ed.): Papermaking Science and Technology: Paper Physics, vol. 16. In: Fapet, O.Y (Ed.) Helsinki, Finland (1998)

Rebai, M., Prat, M.: Scale effect and two-phase flow in a thin hydrophobic porous layer. Application to water transport in gas diffusion layers of PEM fuel cells. J. Power Sour. **192**, 534–543 (2009)

Sarrot,V., Prat, M.: Hyperslow drainage in a porous medium. Influence of retention curve. Adv. Water Resour. **33**, 987–996 (2010)

Satik, C., Yortsos, Y.: A pore-network study of bubble growth in porous media driven by heat transfer. ASME J. Heat Transf. **118**, 455–462 (1996)

Squires, T.M., Quakes, S.R.: Microfluidics : fluid physics at the nanoliter scale. Rev. Mod. Phys. **77**, 977 (2005)

Stauffer, F., Kong, X.Z., Kinzelbach, W.: A stochastic model for air injection into saturated porous media. Adv. Water Resour. **32**(8), 1180–1186 (2009)

Tirunarayanan, M.A., Ramachandran, A.: Correlation of isothermal pressure drop in rectangular ducts. In Proceedings of Australasian Conference on Hydraulics Fluid Mechanics, 2th, University of Auckland, pp. A213–A230 (1965)

Vedvik, A., Wagner, G., Oxaal, U., Feder, J., Meakin, P., Jossang, T.: Fragmentation transition for invasion percolation in hydraulic gradients. Phys. Rev. Lett. **80**(14), 3065–3068 (1998)

Wilkinson, D., Willemsen, J.F.: Invasion percolation: a new form of percolation theory. J. Phys. A **16**, 3365–3376 (1983)

Wong, H., Morris, S., Radke, C.J.: Two dimensional menisci in nonaxisymmetric capillaries. J. Colloid Interface Sci. **148**(1), 284–288 (1992a)

Wong, H., Morris, S., Radke, C.J.: Three dimensional menisci in polygonal capillaries. J. Colloid Interface Sci. **148**(2), 317–336 (1992b)
Wong, H., Radke, C.J., Morris, S.: The motion of long bubbles in polygonal capillaries. Part 1. thin films. J. Fluid Mech. **292**, 71–94 (1995a)
Wong, H., Radke, C.J., Morris, S.: The motion of long bubbles in polygonal capillaries. Part 2 drags, fluid pressure and fluid flow. J. Fluid Mech. **292**, 95–110 (1995b)
Yuan, H.H., Swanson, B.F.: Resolving pore-space characteristics by rate-controlled porosimetry. SPE-FE **4**(1), 17–24 (1989)